Journal of Materials Chemistry A

ROYAL SOCIETY OF CHEMISTRY

PAPER

View Article Online
View Journal | View Issue

Cite this: J. Mater. Chem. A, 2024, 12, 21350

Modulating electrolyte solvation for high-performance aqueous zinc–sulfur batteries†

Tino S. Thomas, Aayushi Prakash Sinha and Debaprasad Mandal *

Rechargeable aqueous zinc/sulfur (Zn/S) batteries are promising candidates for large-scale energy storage applications owing to their high specific capacity and energy density with additional advantages of zinc and sulfur being abundant and cost-effective. However, practical application is impeded by the poor reversibility of the sulfur cathode and parasitic reactions at the Zn anode, limiting their capacity and cycling life. To address these challenges, an aqueous hybrid electrolyte comprising dimethylacetamide (DMA) as a high-donor number organic cosolvent and ZnI_2 as an additive was developed. The designed hybrid electrolyte helps in facile sulfur conversion and efficiently suppresses the HER and corrosion by reconstructing the solvation shell of zinc ions, thereby facilitating uniform Zn deposition. The designed Zn/S battery exhibits improved electrode reversibility with a specific capacity of 1453 mA h g^{-1} at 0.1 A g^{-1} and 72% capacity retention at 5 A g^{-1} over 300 cycles. The DMA-modified electrolyte presents a novel approach for utilizing high donor-number solvents to mitigate water-induced side reactions in other aqueous metal–sulfur batteries.

Received 2nd May 2024
Accepted 5th July 2024

DOI: 10.1039/d4ta03061c

rsc.li/materials-a

Introduction

Advancements in the energy sector for developing portable devices and electric vehicles have stimulated extensive demand for high energy-density energy storage devices.[1,2] In this regard, rechargeable aqueous batteries are promising candidates owing to their advantages of safety, cost-effectiveness, and high ionic conductivity compared to non-aqueous electrolytes; however, a narrow electrochemical stability window (1.23 V), decomposition of water and hydrogen evolution reactions (HERs) pose challenges.[3–6]

Aqueous sulfur batteries have gained importance in recent years owing to the high theoretical capacity of sulfur (1675 mA h g^{-1}), cost-effectiveness, and abundant reserves.[7–9] In this regard, aq. Zn/S batteries can be potential candidates for high energy density storage devices. Zn metal provides a high theoretical capacity of 820 mA h g^{-1}, a low redox potential of −0.76 V *vs.* SHE, abundant reserves, low hydrogen evolution, and high compatibility with aqueous electrolytes.[10–13] Additionally, the sulfur cathode in an aqueous Zn/S battery offers the advantage of negligible polysulfide shuttling due to the solid–solid conversion of S_8 to ZnS and *vice versa*, which is infamous for poor performance in Li-ion/S or Na-ion/S batteries.[14–16] Nevertheless, direct solid–solid conversion of sulfur causes sluggish kinetics, leading to poor cycling performance of aqueous Zn/S batteries (AZSBs).[17] Besides, the poor wettability of the sulfur cathode in an aqueous electrolyte hinders the zinc-ion mobility at the cathode/electrolyte interface, leading to high polarization.[18] Apart from this, over-oxidation of sulfur to sulfate occurs during charging, leading to active material loss.[19] Additionally, zinc metal is prone to dendritic growth and HER in aqueous electrolytes, which eventually result in low battery life.[20,21] Therefore, to address these issues, strategies that would simultaneously stabilize the anode and enhance the sulfur conversion kinetics at the cathode are of great importance.

In this regard, some progress has been made on the sulfur cathode by utilizing redox mediators such as iodine (I_2) or I_3^- as an electrolyte additive to improve the direct solid–solid conversion kinetics of the sulfur cathode and enhance battery performance.[22,23] However, a nonpolar iodine catalyst is sparingly soluble in water, and I_2 and I_3^- react with Zn–metal to accelerate the corrosion of the Zn anode, compromising Zn/S battery performance.[24–26] Moreover, water molecules in aq. electrolyte forms a solvation shell with zinc ions to form $[Zn(H_2O)_6]^{2+}$, and this solvation shell requires higher energy to separate zinc ions from water molecules, causing the HER to occur.[27,28] HER induces corrosion by generating OH^- locally and could react with Zn-ion to form passivating corrosion products of $Zn(OH)_2$, which becomes competitive with the Zn plating process during charging with the following equations:[29]

$$Zn \rightarrow Zn^{2+} + 2e^- \quad (1)$$

$$2H_2O + 2e^- \rightarrow H_2\uparrow + 2OH^- \quad (2)$$

$$2OH^- + Zn^{2+} \rightarrow Zn(OH)_2\downarrow \quad (3)$$

Department of Chemistry, Indian Institute of Technology Ropar, Punjab 140001, India. E-mail: dmandal@iitrpr.ac.in

† Electronic supplementary information (ESI) available. See DOI: https://doi.org/10.1039/d4ta03061c

To circumvent these issues, organic cosolvents with high donor numbers can play a crucial role by competing for the solvation of the zinc ion, preventing the formation of water clusters surrounding Zn ions, and inhibiting the HER at the Zn-anode.[30] Additionally, organic cosolvents have better wettability to sulfur cathode compared to water and facilitate the charge transfer process at the electrode/electrolyte interface.[22,31]

Herein, we propose an efficient strategy for improving the stability of the zinc metal anode as well as faster sulfur conversion kinetics at the cathode in aqueous electrolytes by modifying the solvation structure using a hybrid electrolyte comprising *N*,*N*-dimethylacetamide (DMA) as a cosolvent and ZnI_2 as an additive (Fig. 1). The hybrid electrolyte consists of zinc triflate and DMA as a cosolvent with zinc iodide as an additive and is denoted as aqueous zinc triflate (AZ)/DMA (D)/zinc iodide (ZnI_2) (AZ/D/ZnI_2). DMA is an economical solvent with a high Gutmann donor number (DN, 27.8 *vs.* 18 for water).[32] High DN of DMA plays a crucial role by preventing the formation of water clusters surrounding Zn-ions competing and reconstructing the zinc ion solvation shell by replacing coordinated water molecules and engaging in solvated zinc-ion shell.[33,34] Thus, the designed hybrid electrolyte (AZ/D/ZnI_2) could successfully suppress the parasitic reactions and prevent zinc dendrite formation and Zn-anode passivation.

Results and discussion

Considering the intrinsic challenges of aq. Zn/S battery, this work aims to explore the stabilization of zinc anode and sulfur cathode in an aq.hybrid electrolyte utilizing a high donor number solvent, DMA. Elemental sulfur (50 wt%) was incorporated into the carbon matrix by applying the melt diffusion method to yield S@AC (detailed in ESI†). The composite was characterized by powder X-ray diffraction (PXRD) and X-ray photoelectron spectroscopy (XPS), and 51% sulfur content was observed by thermogravimetric analysis (TGA), indicating the successful incorporation of sulfur into the carbon (Fig. S1a–c (ESI)†).

After the successful incorporation of sulfur into the carbon matrix, the electrolyte was optimized with different ratios of DMA/water, where 20/80 is denoted as DMA-20, 40/60 is denoted as DMA-40 and 60/40 is denoted as DMA-60. The advantages offered by these hybrid electrolytes can be elucidated by understanding the role of DMA in suppressing free water activity. As a cosolvent, DMA can achieve the reconstruction of the Zn^{2+} ion solvation shell.

The interaction of DMA with free water molecules was analyzed by FT-IR, and with increasing DMA concentration, the O–H stretching peak shifted towards a higher wavenumber due to the disruption of the abundant hydrogen bonding network in bulk water. Moreover, the stretching peak of –C=O of DMA exhibits a red shift owing to the hydrogen bonds between water and DMA molecules (Fig. 2a). This was further supported by the ^{1}H- and ^{13}C-NMR of the DMA–water mixture in the presence of 2 M $Zn(OTf)_2$ in D_2O. The peak for H_2O in ^{1}H NMR shifted from 4.67 ppm (H_2O) to 4.73 ppm (DMA-40), while for DMA, the carbonyl peak in ^{13}C NMR shifted from 169.24 ppm (DMA) to 172.96 ppm (DMA-40), highlighting the interaction of DMA with water molecules as correlated in FT-IR (Fig. 2b, S2a and b (ESI†)).

Because electrolyte wettability on the sulfur cathode is crucial for improving the cathode/electrolyte interface for zinc ion mobility in the cathode and for facile electrode kinetics, the wettability of the sulfur cathode was evaluated using a dynamic water contact angle (WCA) with the electrolytes. The change in WCA was recorded for up to 3 minutes (Fig. S3, SI†). Without DMA, the AZ/ZnI_2 electrolyte exhibited a WCA of 116.5°, which drastically decreased to 26.8° for the AZ/D/ZnI_2 hybrid electrolyte. The improved wettability induced by the DMA-modified hybrid electrolyte promotes better electrolyte percolation into the sulfur cathode matrix and reduces the surface free energy for improved zinc ion mobility (Fig. S4 (ESI†)). Notably, superior wettability was also observed in the DMA–water mixture while

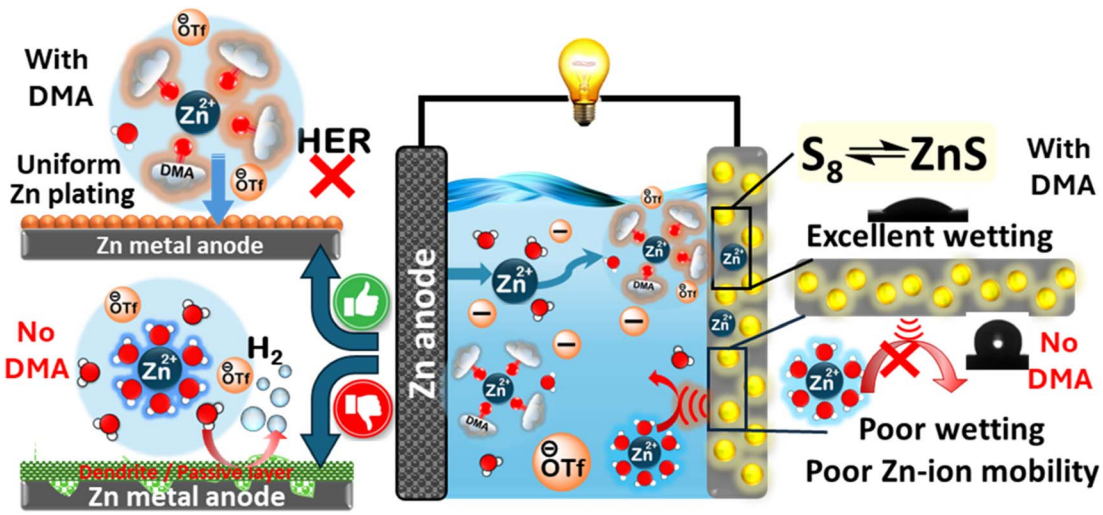

Fig. 1 Designed Zn/S battery with *N*,*N*-dimethylacetamide (DMA) as a cosolvent.

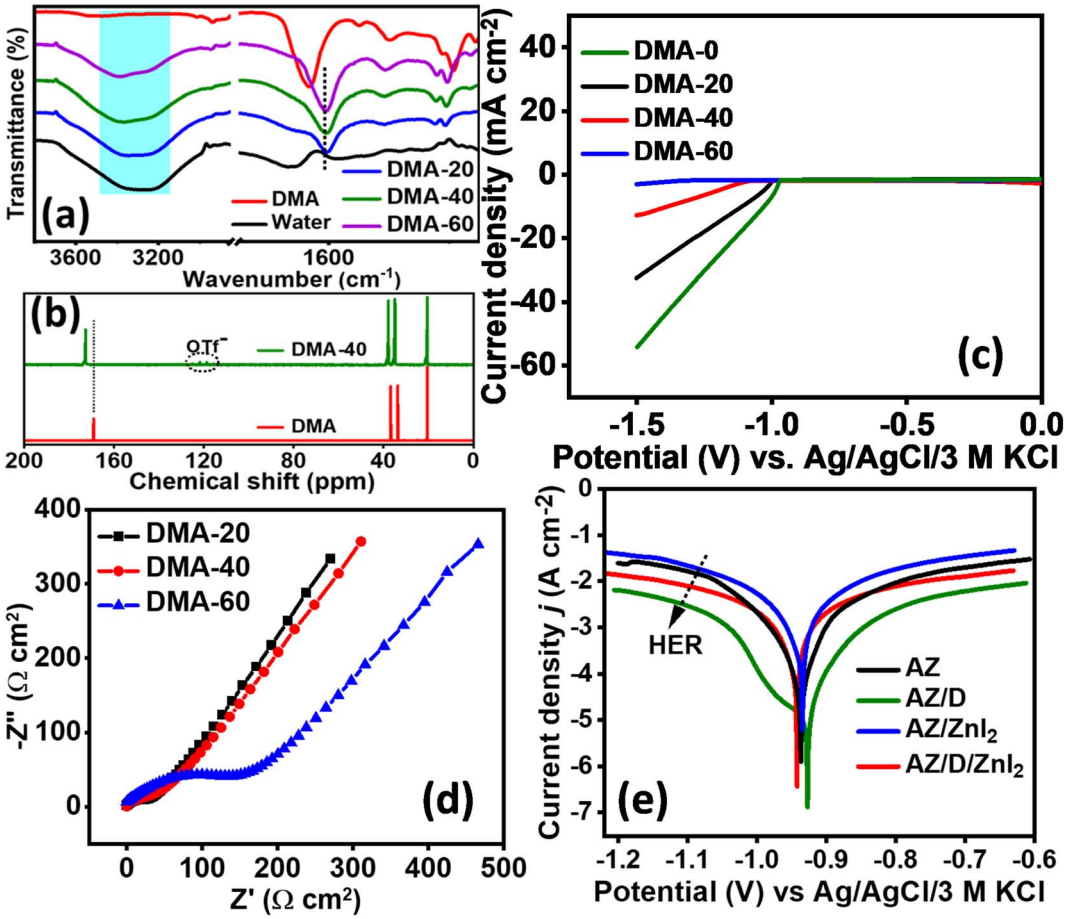

Fig. 2 (a) FT-IR spectra of different DMA–water solutions. (b) ^{13}C-NMR of different DMA–water solutions containing $Zn(OTf)_2$. (c) LSV curves of different DMA–water electrolytes at a scan rate of 10 mV s^{-1}, and (d) corresponding EIS spectra using glassy carbon, Ag/AgCl/3 M KCl and Pt wire as working, reference, and counter electrodes, respectively. (e) Linear polarization of different electrolytes at a scan rate of 1 mV s^{-1} using zinc foil, Ag/AgCl/3 M KCl and Pt wire as working, reference, and counter electrodes, respectively.

soaking sulfur powder in water, DMA, and DMA-40 (Fig. S5 (ESI†)). The use of organic solvents as electrolytes poses the challenge of being flammable and unsafe. Because DMA was used as a cosolvent, the flammability was tested to understand the advantages of our hybrid electrolyte. As depicted in Fig. S6 (ESI†), the separator soaked in DMA instantly caught fire, whereas the separator soaked in hybrid electrolyte AZ/D/ZnI_2 with DMA-40 was nonflammable.

To assess the ability of electrolytes to minimize the HER, electrochemical studies were conducted with 2 M $Zn(OTf)_2$ in DMA–water (AZ/D) by recording the linear sweep voltammogram (LSV) in a three-electrode system using glassy carbon (ϕ 3 mm), Ag/AgCl/3 M KCl and Pt wire as working, reference, and counter electrodes, respectively. The effect of DMA in inhibiting the HER is evident from the LSV in Fig. 2c, where the HER overpotential increased with a higher DMA content from 20 to 60%, indicating the suppression of H_2 generation, and DMA-60 exhibited the maximum suppression, as listed in Table S1 (ESI†). Similarly, the EIS spectra show a higher R_{ct} value, indicating better corrosion suppression, as observed with an increase in DMA concentration (Fig. 2d). However, the increase in R_{ct} value would be detrimental to Zn^{2+} ion mobility. Further, solution resistance R_s was determined by EIS fitting, as listed in Table S2 (ESI†). Hence, an optimal DMA-to-water ratio of 40 : 60 v/v (DMA-40) was adopted for further studies.

Additionally, linear polarization (LP) of AZ/D/ZnI_2 was recorded using zinc foil, Ag/AgCl/3 M KCl and Pt wire as working, reference, and counter electrodes, respectively, to assess the effect of DMA in minimizing HER and corrosion protection. As illustrated in Fig. 2e, a notable decrease in corrosion current density (i_{corr}) by 2.5 times was observed for AZ/D/ZnI_2 (4.16 mA cm^{-2}) compared to AZ/ZnI_2 electrolyte (10.47 mA cm^{-2}), indicating better corrosion resistance. The cathodic current corresponded to HER increases upon the addition of ZnI_2, whereas a decrease was observed in the cathodic current in the electrolyte containing DMA. This trend was consistent with the EIS spectra, where higher R_{ct} values were observed in the case of DMA containing electrolytes (Fig. S7 (ESI†)), highlighting the role of DMA in enhancing HER overpotential and minimizing corrosion. Besides, a decreased anodic current density corresponds to hindered zinc dissolution and implies the suppression of zinc ion mobility, impeding

the battery performance. In the hybrid electrolyte (AZ/D/ZnI_2), alongside HER minimization, the Zn-ion ionic mobility remains unaffected, rendering the system efficient for battery operation. Therefore, DMA-40 containing a hybrid electrolyte (AZ/D/ZnI_2) effectively suppresses free water activity by increasing the HER overpotential, leading to the minimization of corrosion, and is further utilized as a model electrolyte for further investigations.

The zinc metal anode is prone to dendritic growth and passivation during cycling, leading to low utilization. Therefore, to assess the hybrid electrolyte in mitigating parasitic reactions and dendrite formation occurring at the anode, Zn//Zn symmetric cells were employed with both aqueous AZ/ZnI_2 and hybrid electrolytes. The suppression of dendrite growth was analyzed by monitoring the voltage hysteresis and morphological changes during the zinc stripping/plating test at a current density of 2 mA cm^{-2} and an areal capacity of 1 mA h cm^{-2}. Voltage hysteresis of the Zn//Zn symmetrical cell with AZ/ZnI_2 electrolyte exhibits fluctuations and a short cycling life of 44 h (Fig. 3a). In contrast, the Zn//Zn symmetrical cell containing AZ/D/ZnI_2 continues to operate a long cycling life of 130 h without any fluctuation or decay (the battery was tested up to 130 h). This confirms that DMA induces a stable voltage profile with a highly reversible Zn plating/stripping process. However, the increase in voltage polarization in the presence of DMA than AZ/ZnI_2 is attributed to the increased viscosity and reduced ionic conductivity of the electrolyte. Additionally, EIS performed at the 10^{th} cycle and at the end of the cycling showed a decrease in charge transfer resistance (R_{ct}) upon cycling in AZ/D/ZnI_2 operated Zn//Zn cell, which may be due to the electrochemical reconstruction of the surface, leading to the formation of a new integrated architecture (Fig. 3b and c, S8 a and b, ESI†).[35] In contrast, an increase in the R_{ct} was observed in AZ/ZnI_2, highlighting the positive impact of DMA on stabilizing the anode/electrolyte interface for the superior lifecycle of AZ/D/ZnI_2 operated Zn//Zn cell.

Post-cycling PXRD analysis of Zn electrodes retrieved from the cell operated with AZ/ZnI_2 electrolyte revealed inhomogeneous Zn deposition, and the XRD patterns matched with the characteristic peaks of corrosion products, such as $Zn_xOTf_y(OH)_{2x-y}\cdot nH_2O$ (Fig. 3d).[31] The peaks at 16.6° and 31.5° correspond to the zinc triflate used in the electrolyte. Surprisingly, the cell operated utilizing AZ/D/ZnI_2 exhibited no additional peaks other than characteristic Zn metal, signifying a homogenous zinc deposition without any side product. Moreover, optical images show a smoother surface for the hybrid electrolyte, indicating the inhibition of corrosion and dendritic growth of the Zn anode (Fig. S9a and b (ESI†)). FESEM of the Zn anode in AZ/ZnI_2 showed a sharp needle-like microstructure due to uneven deposition during cycling, which caused fluctuations and a short cycle life, while the Zn anode in AZ/D/ZnI_2 showed smoother morphology, suggesting uniform deposition during stripping/plating (Fig. 3e and f). Subsequently, full-cell batteries were assembled utilizing Zn foil as anode and S@AC as a cathode in AZ/ZnI_2 and AZ/D/ZnI_2 electrolytes, and the battery performance was assessed by conducting cyclic voltammetry (CV) and galvanostatic charge–discharge (GCD) analysis. Initially, to understand the effect of DMA, the CV was recorded at a scan rate of 0.2 mV s^{-1}. A well-defined redox behavior corresponding to the sulfur redox reaction with one cathodic and one anodic peak was observed, as shown in Fig. 4a, wherein the redox pairs at 0.3 V and 1.3 V corresponded to the reduction of S_8 to ZnS and the oxidation of ZnS to S_8, respectively, indicating the reversibility of the process. A decrease in cathodic current corresponding to sulfur reduction at 0.3 V in the hybrid

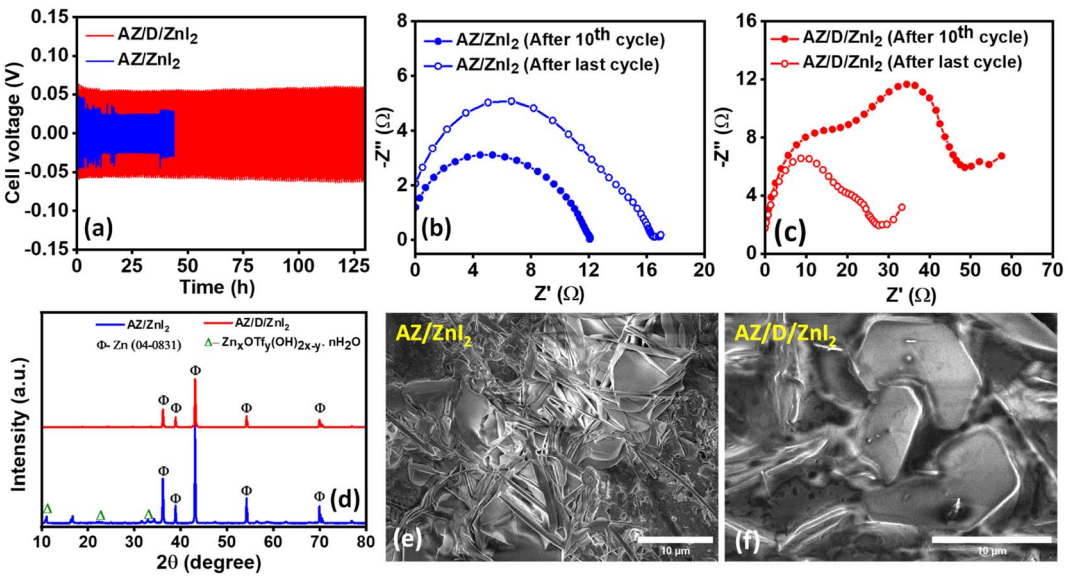

Fig. 3 (a) Zn stripping/plating of Zn//Zn symmetric cells in AZ/ZnI_2 and AZ/D/ZnI_2 electrolytes at 2 mA cm^{-2} and 1 mA h cm^{-2}. EIS spectra of Zn//Zn symmetric cells (cycled at 10 cycles and at the last cycle at 2 mA cm^{-2}) in (b) AZ/ZnI_2, and (c) AZ/D/ZnI_2 electrolyte. (d) XRD spectra of zinc electrodes after Zn//Zn symmetrical cycling in AZ/ZnI_2 and AZ/D/ZnI_2 electrolytes. FESEM of Zn after Zn//Zn symmetrical cycling in (e) AZ/ZnI_2 and (f) AZ/D/ZnI_2 electrolytes.

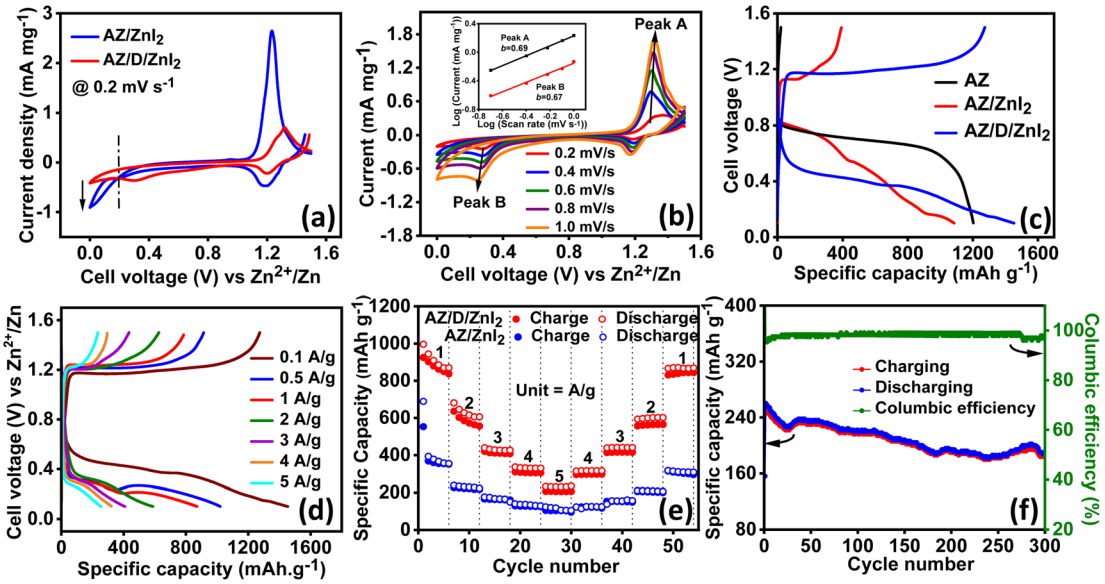

Fig. 4 (a) CV curves of the Zn/S batteries in AZ/ZnI_2 and AZ/D/ZnI_2 electrolytes at 0.2 mV s^{-1}. (b) Corresponding CV curves in AZ/D/ZnI_2 at different scan rates. (c) Specific capacity plot of the battery operated with AZ, AZ/ZnI_2, and AZ/D/ZnI_2 electrolytes at 0.1 A g^{-1}. (d) GCD curves of the Zn/S battery in AZ/D/ZnI_2 at different current densities. (e) Rate performance of the Zn/S battery in AZ/ZnI_2 and AZ/D/ZnI_2 electrolytes. (f) Long-term cycling performance of the Zn/S batteries in AZ/D/ZnI_2 at 5 A g^{-1}.

electrolyte AZ/D/ZnI_2 suggests improved stability and increased HER overpotential in the presence of DMA. In contrast, CV in AZ/ZnI_2 containing Zn/S battery lacks a well-defined reduction peak, which may be due to H_2 evolution. Additionally, the CV studies with AZ/D/ZnI_2 at various scan rates ranging from 0.2 mV s^{-1} to 1 mV s^{-1}, as shown in Fig. 4b, reveal well-defined redox peaks with negligible changes in peak potential and shape with increasing scan rate, indicating good stability of the cathode. Analysis of the plot of $\log i$ *vs.* $\log v$ from the cyclic voltammogram using the equation $i = av^b$ (i = peak current and v = scan rate); the slope (b) was found to be 0.69 for peak A and 0.67 for peak B (Fig. S10 (ESI†)), suggesting a highly reversible and diffusion-controlled redox process in AZ/D/ZnI_2 electrolyte.[22,36] To assess the practical viability of the designed Zn/S battery, GCD studies were conducted by employing different electrolytes. Due to the improved Zn-ion mobility at the electrode/electrolyte interface, the battery utilizing AZ/D/ZnI_2 achieved a high initial discharge capacity of 1453 mA h g^{-1} at 0.1 A g^{-1} with an energy density of 582 W h kg^{-1} with respect to the weight of S, which is better than or comparable to the recent literature (Table S3 (ESI†)). In contrast, batteries containing AZ and AZ/ZnI_2 electrolytes delivered 1203 and 1086 mA h g^{-1} at 0.1 A g^{-1}, respectively (Fig. 4c). However, batteries devoid of DMA exhibited inefficient charging performance. Further, the battery delivered reversible capacities of 1453, 1020, 938, 592, 410, 323, and 254 mA h g^{-1} across current densities ranging from 0.1 A g^{-1} to 5 A g^{-1} (Fig. 4d). The rate capability of the battery in AZ/D/ZnI_2 electrolyte was then evaluated (Fig. 4e). At 1 A g^{-1} current density, the battery delivered reversible capacity, which decreased with an increasing current density of up to 5 A g^{-1}. Upon reversing the current density back to 1 A g^{-1}, the capacity recovers almost to its initial capacity, demonstrating excellent rate capability and stability. Long-term stability analysis in Fig. 4f revealed that the Zn/S battery maintained good long-term stability in AZ/D/ZnI_2 electrolyte at 5 A g^{-1} for 300 cycles, with a capacity retention of 72%. In comparison, the battery utilizing AZ and AZ/ZnI_2 electrolytes delivered inferior capacity as well as rate capability and poor long-term performance (Fig. 4c, e and S11 (ESI†)). Additionally, to understand the influence of DMA concentration on battery performance, GCD was performed at 1 A g^{-1} with two batteries assembled by utilizing AZ/D(40)/ZnI_2 and AZ/D(60)/ZnI_2 electrolytes. The battery with DMA-40 delivered a three-fold higher discharge capacity compared to DMA-60 (Fig. S12 (ESI†)).

To understand the various intermediates during solid–solid conversion, potential dependent XPS analyses were performed on the retrieved cathodes by stopping the battery at different charge–discharge potentials. As depicted in Fig. 5a, prior to discharging (Point A), the battery exhibited peaks corresponding to sulfur at 163.8 eV and 164.9 eV for $S2p_{3/2}$ and $S2p_{1/2}$, respectively, while the peaks of the triflate anion appeared at 168.9 eV and 170.1 eV for $S2p_{3/2}$ and $S2p_{1/2}$ respectively. Upon discharging to 0.35 V (Point B), the S_8 peak started reducing gradually, while the ZnS peak at 161.9 eV and 163.1 eV for $S2p_{3/2}$ and $S2p_{1/2}$ began to emerge, respectively. Upon complete discharge at Point C, the ZnS peak became predominant, with minimal unutilized sulfur remaining. Reversing the cycle and charging the battery to 1.25 V (Point D) led to the reappearance of the sulfur peaks at 163.7 eV and 164.9 eV, while the ZnS peak entirely disappeared upon charging to 1.5 V (Point E), implying facile conversion between S and ZnS. Moreover, no peaks corresponding to polysulfides were detected during cycling. Further, Raman spectra showed similar observations, as shown in Fig. 5b. The peaks at 146 cm^{-1}, 218 cm^{-1} and 470 cm^{-1}

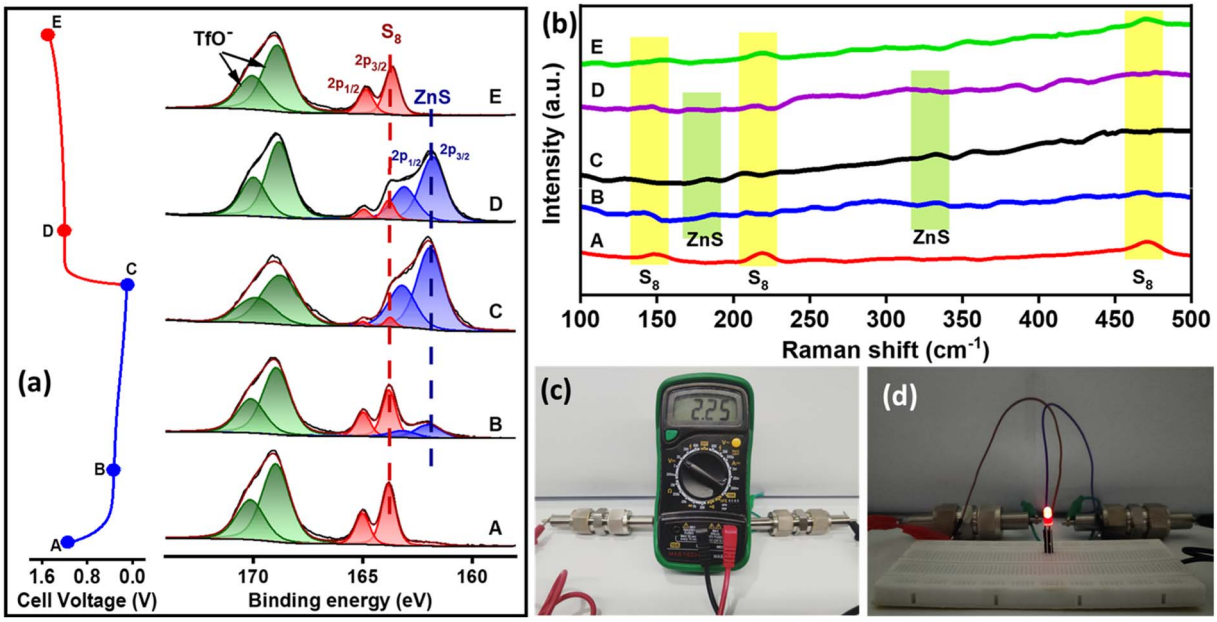

Fig. 5 (a) XPS and (b) Raman spectra of S@AC at different charge–discharge voltages. (c) Obtained OCP by connecting two Zn/S batteries. (d) Powering of 1.8 V red LED by two Zn/S battery.

corresponding to S_8 gradually diminished during discharge, and the peaks for ZnS at 184 cm^{-1} and 332 cm^{-1} were observed when the battery was fully discharged. Upon charging, the ZnS peak started to diminish, and only sulfur peaks were observed when the battery was fully charged, suggesting a one-step solid–solid conversion of the S cathode in AZ/D/ZnI_2 hybrid electrolyte. Additionally, to demonstrate the practical utility of our designed hybrid electrolyte, two Zn/S batteries in series were assembled with AZ/D/ZnI_2 delivered an OCP of 2.25 V and were able to successfully power a red LED (1.8 V), as shown in Fig. 5b and c.

Conclusions

In summary, we demonstrated the utilization of *N*,*N*-dimethylacetamide as a cosolvent in the preparation of a hybrid electrolyte, AZ/D/ZnI_2, for rechargeable aqueous zinc–sulfur batteries. Electrochemically and spectroscopically, we demonstrated a significant reduction in free water activity, leading to enhanced stability of the Zn/S battery against parasitic reactions, such as hydrogen evolution and electrode corrosion. Moreover, DMA as a cosolvent improved the wettability of the electrolyte on the sulfur cathode and provided homogenous stripping/plating on the Zn anode, resulting in enhanced compatibility at the electrode/electrolyte interface. The resultant battery employing DMA-40 delivered a high initial discharge capacity of 1453 mA h g^{-1}@0.1 A g^{-1} and a high energy density of 582 W h kg^{-1}. Notably, the capacity retention reaches 72% with high cycling stability for 300 cycles@5 A g^{-1}. Furthermore, as a demonstration of practical utility, the designed aqueous Zn/S batteries successfully powered a red LED. Our findings suggest that the use of high donor number solvents, such as DMA, could play a vital role in stabilizing the cathode/electrolyte interface and enabling efficient utilization of anodes for other metal–sulfur batteries with the advantages of low-cost and nonflammability.

Data availability

The data supporting this article have been included as part of the ESI.†

Author contributions

Tino S. Thomas: conceptualization, methodology, software, data curation, writing – original draft, visualization, investigation, formal analysis. Aayushi Prakash Sinha: methodology, data curation, formal analysis, writing – review & editing, software. Debaprasad Mandal: conceptualization, visualization, writing – review & editing, supervision, funding acquisition.

Conflicts of interest

The authors declare no competing financial interests.

Acknowledgements

D. Mandal acknowledges SERB (CRG/2023/004666) and CSIR (02(0436/21/EMR-II)) for funding support. Tino S. Thomas (DEC18-114672) thanks UGC for fellowship, and Aayushi P Sinha thanks DST for Inspire Fellowship (DST/INSPIRE/03/2019/000968). The authors thank the CRF facility, IIT Ropar for XPS and FESEM analysis. AMRC, IIT Mandi is gratefully acknowledged for providing Raman facility.

References

1 F. Wu, J. Maier and Y. Yu, *Chem. Soc. Rev.*, 2020, **49**, 1569–1614.
2 J. Deng, C. Bae, A. Denlinger and T. Miller, *Joule*, 2020, **4**, 511–515.
3 Y. Liang and Y. Yao, *Nat. Rev. Mater.*, 2023, **8**, 109–122.
4 D. Chao, W. Zhou, F. Xie, C. Ye, H. Li, M. Jaroniec and S.-Z. Qiao, *Sci. Adv.*, 2020, **6**, eaba4098.
5 Y. Shen, B. Liu, X. Liu, J. Liu, J. Ding, C. Zhong and W. Hu, *Energy Storage Mater.*, 2021, **34**, 461–474.
6 H. Zhang, X. Liu, H. Li, I. Hasa and S. Passerini, *Angew. Chem., Int. Ed.*, 2021, **60**, 598–616.
7 J. Liu, W. Zhou, R. Zhao, Z. Yang, W. Li, D. Chao, S.-Z. Qiao and D. Zhao, *J. Am. Chem. Soc.*, 2021, **143**, 15475–15489.
8 S. Yun, S. H. Park, J. S. Yeon, J. Park, M. Jana, J. Suk and H. S. Park, *Adv. Funct. Mater.*, 2018, **28**, 1707593.
9 C. Wei, Y. Wang, Z. Ding, T. Fang, J. Song, Y. Zhang, S. Lv, X. Liu and X. Tang, *Adv. Funct. Mater.*, 2023, **33**, 2212644.
10 W. Li, K. Wang and K. Jiang, *Adv. Sci.*, 2020, **7**, 2000761.
11 X. Chen, X. Xie, P. Ruan, S. Liang, W.-Y. Wong and G. Fang, *ACS Energy Lett.*, 2024, 2037–2056, DOI: **10.1021/acsenergylett.4c00450**.
12 C. Feng, X. Jiang, Q. Zhou, T. Li, Y. Zhao, Z. Niu, Y. Wu, H. Zhou, M. Wang, X. Zhang, M. Chen, L. Ni, G. Diao and Y. Wei, *J. Mater. Chem. A*, 2023, **11**, 18029–18045.
13 Z. Yang, F. Lai, Q. Mao, C. Liu, R. Wang, Z. Lu, T. Zhang and X. Liu, *Adv. Mater.*, 2024, **36**, 2311637.
14 H. Zhang, Z. Shang, G. Luo, S. Jiao, R. Cao, Q. Chen and K. Lu, *ACS Nano*, 2022, **16**, 7344–7351.
15 M. Kumar, A. K. Padhan, D. Mandal and T. C. Nagaiah, *Energy Storage Mater.*, 2022, **45**, 1052–1061.
16 C. Yang, L. Suo, O. Borodin, F. Wang, W. Sun, T. Gao, X. Fan, S. Hou, Z. Ma, K. Amine, K. Xu and C. Wang, *Proc. Natl. Acad. Sci. U. S. A.*, 2017, **114**, 6197–6202.
17 W. Wu, S. Wang, L. Lin, H.-Y. Shi and X. Sun, *Energy Environ. Sci.*, 2023, **16**, 4326–4333.
18 Y. Zhao, D. Wang, X. Li, Q. Yang, Y. Guo, F. Mo, Q. Li, C. Peng, H. Li and C. Zhi, *Adv. Mater.*, 2020, **32**, 2003070.
19 G. Chang, J. Liu, Y. Hao, C. Huang, Y. Yang, Y. Qian, X. Chen, Q. Tang and A. Hu, *Chem. Eng. J.*, 2023, **457**, 141083.
20 J. Li, Z. Cheng, Z. Li and Y. Huang, *Mater. Horiz.*, 2023, **10**, 2436–2444.
21 Y. Zhang, A. Amardeep, Z. Wu, L. Tao, J. Xu, D. J. Freschi and J. Liu, *Adv. Sci.*, 2024, 2308580, DOI: **10.1002/advs.202308580**.
22 M. Yang, Z. Yan, J. Xiao, W. Xin, L. Zhang, H. Peng, Y. Geng, J. Li, Y. Wang, L. Liu and Z. Zhu, *Angew. Chem., Int. Ed.*, 2022, **61**, e202212666.
23 D. Liu, B. He, Y. Zhong, J. Chen, L. Yuan, Z. Li and Y. Huang, *Nano Energy*, 2022, **101**, 107474.
24 P. Hei, Y. Sai, C. Liu, W. Li, J. Wang, X. Sun, Y. Song and X.-X. Liu, *Angew. Chem., Int. Ed.*, 2024, **63**, e202316082.
25 H. Chen, X. Li, K. Fang, H. Wang, J. Ning and Y. Hu, *Adv. Energy Mater.*, 2023, **13**, 2302187.
26 J. Zhang, Q. Dou, C. Yang, L. Zang and X. Yan, *J. Mater. Chem. A*, 2023, **11**, 3632–3639.
27 M. Li, Z. Li, X. Wang, J. Meng, X. Liu, B. Wu, C. Han and L. Mai, *Energy Environ. Sci.*, 2021, **14**, 3796–3839.
28 S. Chen, D. Ji, Q. Chen, J. Ma, S. Hou and J. Zhang, *Nat. Commun.*, 2023, **14**, 3526.
29 Y. Yang, C. Liu, Z. Lv, H. Yang, X. Cheng, S. Zhang, M. Ye, Y. Zhang, L. Chen, J. Zhao and C. C. Li, *Energy Storage Mater.*, 2021, **41**, 230–239.
30 J. Luo, L. Xu, Y. Zhou, T. Yan, Y. Shao, D. Yang, L. Zhang, Z. Xia, T. Wang, L. Zhang, T. Cheng and Y. Shao, *Angew. Chem., Int. Ed.*, 2023, **62**, e202302302.
31 Y. Guo, R. Chua, Y. Chen, Y. Cai, E. J. J. Tang, J. J. N. Lim, T. H. Tran, V. Verma, M. W. Wong and M. Srinivasan, *Small*, 2023, **19**, 2207133.
32 H. Shin, M. Baek, A. Gupta, K. Char, A. Manthiram and J. W. Choi, *Adv. Energy Mater.*, 2020, **10**, 2001456.
33 M. Li, X. Feng, J. Yin, T. Cui, F. Li, J. Chen, Y. Lin, X. Xu, S. Ding and J. Wang, *J. Mater. Chem. A*, 2023, **11**, 25545–25554.
34 Y. Wang, Z. Wang, W. K. Pang, W. Lie, J. A. Yuwono, G. Liang, S. Liu, A. M. D. Angelo, J. Deng, Y. Fan, K. Davey, B. Li and Z. Guo, *Nat. Commun.*, 2023, **14**, 2720.
35 J. Ma, S. Ni, J. Zhang, X. Yang and L. Zhang, *Phys. Chem. Chem. Phys.*, 2015, **17**, 21442–21447.
36 J. Wang, J. Polleux, J. Lim and B. Dunn, *J. Phys. Chem. C*, 2007, **111**, 14925–14931.